



**La<sub>3</sub>B<sub>14</sub>–: An Inverse Triple-Decker Lanthanide Boron Cluster**

Journal:	<i>ChemComm</i>
Manuscript ID	CC-COM-05-2019-003807.R1
Article Type:	Communication

SCHOLARONE™  
Manuscripts

## COMMUNICATION

**La<sub>3</sub>B<sub>14</sub><sup>-</sup>: An Inverse Triple-Decker Lanthanide Boron Cluster**

Received 00th January 20xx,  
Accepted 00th January 20xx

Teng-Teng Chen,<sup>†</sup> Wan-Lu Li,<sup>‡</sup> Wei-Jia Chen,<sup>a</sup> Jun Li<sup>\*bc</sup> and Lai-Sheng Wang<sup>\*a</sup>

DOI: 10.1039/x0xx00000x

**We report the observation of the first inverse triple-decker complex in a tri-lanthanide-doped boron cluster. Photoelectron spectroscopy of La<sub>3</sub>B<sub>14</sub><sup>-</sup> reveals well-resolved photodetachment transitions. Quantum chemical studies show that the most stable structure of the La<sub>3</sub>B<sub>14</sub><sup>-</sup> cluster exhibits a tilted La–B<sub>8</sub>–La–B<sub>8</sub>–La inverse triple-decker structure with two conjoined B<sub>8</sub> rings sharing a pair of B atoms due to strong inter-layer B–B bonding. The tilted structure enhances both B–B and B–La bonding, resulting in a highly stable inverse triple-decker structure. Theoretical calculations further show that multi-decker conjoined structures are viable as a new class of 1D lanthanide boron nanostructures.**

Boron displays many allotropes with complex crystal structures and super-hard properties because of its electron deficiency and the strong covalent B–B bonding.<sup>1,2</sup> Boron can also form a variety of metal boride materials with important potential industrial applications, ranging from super-hard metal borides and the superconducting MgB<sub>2</sub> to boride materials with ultra-high magnetic fields and ultra-high thermal conductivity.<sup>3–5</sup> Nanoclusters of boron have also been shown to display a diverse range of interesting stable structures and multi-center chemical bonding.<sup>6–10</sup> Joint experimental and theoretical studies in the past decade on size-selected boron clusters have revealed planar (2D) structures leading to the discovery of graphene-like planar structures (borophenes), fullerene-like cage structures (borospherenes), and nanotubular structures.<sup>6–13</sup> Metal-doped boron clusters have led to a new direction in the study of boron nanoclusters, resulting in the discovery of metal-centered molecular wheels, half-sandwich structures, possibilities of metallo-borophenes, and nanotubular drum-like structures.<sup>14–19</sup> Most recently, a new class of inverse-sandwich lanthanide boride clusters involving monocyclic and aromatic B<sub>n</sub> rings (M–B<sub>n</sub>–M, n = 7–9) have been uncovered via joint photoelectron spectroscopy (PES) and quantum chemistry calculations.<sup>20,21</sup>

These exciting findings immediately lead to the question whether triple-decker or even multi-decker lanthanide boride clusters would be possible.

Triple-decker complexes (L–M–L–M–L, L = aromatic ligands) represent a class of interesting organometallic compounds important in organic and inorganic syntheses, as well as building blocks for molecular architectures.<sup>22–25</sup> The first triple-decker transition-metal complex was synthesized in 1972,<sup>26</sup> followed by electronic structure studies and the syntheses of a series of new triple-decker compounds.<sup>27–30</sup> In the past four decades, a variety of triple-decker complexes have been synthesized with different aromatic ligands and d-/f-metal atoms, which can be potential one-dimensional (1D) magnetic materials and molecular information storage media.<sup>25,31–34</sup> However, inverse triple-decker (M–L–M–L–M) or multi-decker lanthanide complexes have not been synthesized.

Here we report the first observation and characterization of a tri-lanthanum-doped boron cluster, La<sub>3</sub>B<sub>14</sub><sup>-</sup>, which is found to possess a tilted inverse triple-decker structure using a joint PES and theoretical investigation. Global minimum searches have shown that the structure can be viewed as two conjoined B<sub>8</sub> rings sharing two B atoms with C<sub>2v</sub> symmetry. Theoretical calculations show that multi-decker La<sub>n</sub>B<sub>6n-4</sub><sup>-</sup> systems with conjoined B<sub>8</sub> rings can form stable 1D lanthanide-boron nanowires. Such novel 1D nanostructures may be viable to be realized experimentally on suitable substrates or found as motifs in new lanthanide borides.

The La<sub>3</sub>B<sub>14</sub><sup>-</sup> cluster was produced using laser-vaporization of a mixed La/<sup>11</sup>B disk target and characterized by a magnetic-bottle PES apparatus (see the Supporting Information for details).<sup>10,35</sup> The photoelectron spectrum of La<sub>3</sub>B<sub>14</sub><sup>-</sup> at 193 nm is shown in Figure 1a, which is well resolved with distinct spectral features, labeled as X, A–H. The X band corresponds to the detachment transition from the ground state of La<sub>3</sub>B<sub>14</sub><sup>-</sup> to that of neutral La<sub>3</sub>B<sub>14</sub>, while the bands at higher binding energies come from detachment transitions to excited states of neutral La<sub>3</sub>B<sub>14</sub>. The overall spectral pattern is relatively simple and well-resolved for such a complicated binary cluster, suggesting a highly stable and symmetric global minimum. Band X is sharp and intense, giving rise to the first vertical detachment energy (VDE) of 2.25 eV for La<sub>3</sub>B<sub>14</sub><sup>-</sup>. The adiabatic detachment energy (ADE) of band X was estimated from its onset to be 2.05 eV, which also represents the electron affinity (EA) of neutral

<sup>a</sup> Department of Chemistry, Brown University, Providence, Rhode Island 02912 (USA). E-mail: Lai-Sheng\_Wang@brown.edu

<sup>b</sup> Department of Chemistry and Key Laboratory of Organic Optoelectronics & Molecular Engineering of Ministry of Education, Tsinghua University, Beijing 100084 (China). E-mail: junli@tsinghua.edu.cn

<sup>c</sup> Department of Chemistry, Southern University of Science and Technology, Shenzhen, Guangdong 518055 (China).

<sup>†</sup> Electronic Supplementary Information (ESI) available.

See DOI: 10.1039/x0xx00000x

<sup>‡</sup> These authors contributed equally to this work.

$\text{La}_3\text{B}_{14}$ . Following an energy gap, band A at 3.15 eV is well separated from other spectral features. Following another energy gap from band A, a congested spectral range ensues from about 3.5 to 4.5 eV. Three bands are labeled, B, C, D, which are likely to contain multiple detachment transitions. Between 4.5 and 6.2 eV, again congested spectral features are observed and four bands, E, F, G, and H, are tentatively identified. The binding energies of all detachment features are given in Table S1. The PES spectral features and the overall spectral pattern of  $\text{La}_3\text{B}_{14}^-$  can serve as an electronic fingerprint that can be used to compare with theoretical calculations to probe its structure, stability, and chemical bonding.

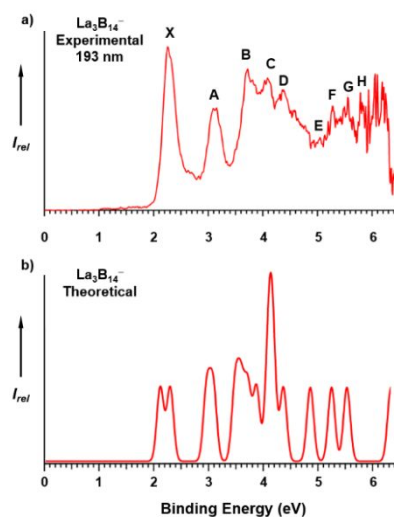


**Figure 1.** a) Photoelectron spectrum of  $\text{La}_3\text{B}_{14}^-$  at 193 nm; b) the simulated spectrum of the tilted triple-decker global minimum of  $\text{La}_3\text{B}_{14}^-$  at the SAOP/TZP level.

The global minimum of  $\text{La}_3\text{B}_{14}^-$  was searched using the TGMIn 2.0 package<sup>36,37</sup> combined with calculations employing the ADF software.<sup>38</sup> We examined more than 1000 structures and found that a tilted inverse triple-decker structure with  $C_{2v}$  symmetry was the global minimum on the potential energy surface, as shown in Figure 2, and the Cartesian coordinates are listed in Table S2. The  $C_{2v}$  structure can be viewed as the fusion of two  $B_8$  monocyclic rings sharing two B atoms. The structural relation between the  $C_{2v}$  global minimum and a perfect La–B<sub>8</sub>–La–B<sub>8</sub>–La triple decker will be discussed later (*vide infra*). Low-lying isomers within 54 kcal/mol of the global minimum are given in Figure S1. The second lowest energy isomer ( $C_1$ ) is found to be 10.92 kcal/mol higher in energy than the  $C_{2v}$  global minimum at the PBE0/TZP level, highlighting the stability of the tilted triple-decker structure. We also calculated the linear La–B<sub>7</sub>–La–B<sub>7</sub>–La triple-decker structure with two  $B_7$  monocyclic rings and found two imaginary frequencies involving the bending modes (tilting) of the two  $B_7$  rings. Furthermore, the energy of this triple-decker structure lies 150 kcal/mol above the  $C_{2v}$  global minimum. Following the imaginary frequencies would lead to the global minimum.

To validate the global minimum of the  $\text{La}_3\text{B}_{14}^-$  cluster, we calculated the first ADE and VDEs of the  $C_{2v}$  tilted triple-decker structure using the PBE and PBE0 methods with the TZP basis

sets. All the calculated detachment channels together with the electron configurations and final state symmetries are compared with the experimental data in Table S1. Each VDE is fitted with a unit-area Gaussian of 0.15 eV width to produce a simulated spectrum, as shown in Figure 1b. The computed first ADE/VDE are 2.12/2.18 eV, in good agreement with the experimental results of 2.05/2.25 eV.

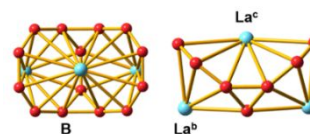


**Figure 2.** The global minimum structure of  $\text{La}_3\text{B}_{14}^-$  ( $C_{2v}$ ,  $^1A_1$ ) with two conjoined  $B_8$  rings: top view (left) and side view (right).  $\text{La}^b$  and  $\text{La}^c$  represent the outer and central La atoms, respectively.

The  $C_{2v}$  tilted triple-decker structure of  $\text{La}_3\text{B}_{14}^-$  has a closed-shell electron configuration and its valence molecular orbitals (MOs) are depicted in Figure S2. Hence, electron detachment from each occupied MO results in one doublet final state (Table S1), yielding a relatively simple photoelectron spectrum. Detachment from the  $24b_2$  HOMO gives rise to a computed VDE of 2.18 eV, whereas detachment from the  $18a_2$  HOMO-1 results in a computed VDE of 2.36 eV. These two detachment channels have closely spaced binding energies, consistent with the intense band X. Detachments from the  $45a_1$  and  $17a_2$  MOs also give rise to two closely spaced VDEs at 3.05 eV and 3.17 eV, respectively, which are well separated from the first two detachment channels, in excellent agreement with band A (experimental VDE of 3.15 eV). Following an energy gap and starting from the  $34b_1$  MO, which gives a computed VDE of 3.58 eV, a series of closely-spaced detachment channels are computed up to 5.7 eV, consistent with the congested PE spectral features beyond band A (Figure 1 and Table S1). Overall, the simulated spectrum from the global minimum of  $\text{La}_3\text{B}_{14}^-$  agrees well with the experimental data, providing considerable credence for the identified tilted triple-decker structure.

The chemical bonding of the tilted triple-decker global minimum of  $\text{La}_3\text{B}_{14}^-$  is analyzed using the adaptive natural density partitioning (AdNDP) method.<sup>39</sup> The AdNDP results reveal that the 52 valence electrons in  $\text{La}_3\text{B}_{14}^-$  can be classified into six categories, as displayed in Figure 3. Eleven two-center two-electron (2c-2e)  $\sigma$  bonds are found, five on each  $B_8$  ring plus one between the two shared boron atoms. There are also two 3c-2e delocalized bonds on the  $B_3$  units shared by the two  $B_8$  rings (Figure 2). There are two 14c-2e bonds with  $\pi$  characters representing delocalized bonding within the two conjoined  $B_8$  rings with little bonding with the La atoms. The remaining 11 multicenter bonds describe various levels of interactions between the conjoined  $B_8$  ligands and the three La atoms in the tilted triple-decker. The three delocalized 15c-2e bonds in the second row represent mainly interactions between the central La atom (labeled as  $\text{La}^c$ ) and the boron framework, involving the  $\text{La}^c$  5d  $\pi$  and 5d  $\delta$  orbitals. The two outer La atoms (labeled as  $\text{La}^b$ ) interact with the fourteen B atoms via six 16c-2e bonds, as depicted in the third row. Different interactions are defined

according to the z-axis along the  $\text{La}^b \dots \text{La}^b$  direction: “+” and “-” represent positive and negative overlaps, respectively. Finally, the two 17c-2e bonds in the fourth row describe bonding between the three La atoms and the boron framework in the tilted triple-decker, with primary interactions involving the two outer  $\text{La}^b$  atoms and the boron framework with some contribution from the central  $\text{La}^c$  atom.

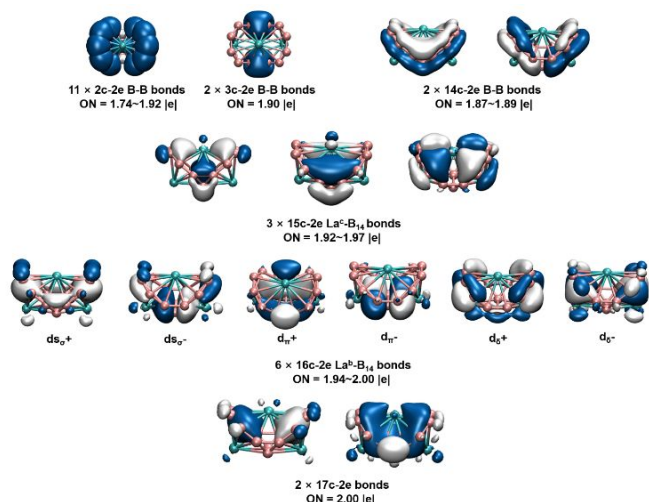


**Figure 3.** AdNDP analyses of the chemical bonding in the tilted inverse triple-decker global minimum of  $\text{La}_3\text{B}_{14}^-$  at the PBE0/TZP level. The occupation number (ON) is given.

Recently, the first inverse sandwich consisting of a  $\text{B}_8$  ring and two La atoms ( $\text{D}_{8h}$   $\text{La}_2\text{B}_8$ ) has been observed. The B–B and B–La bond distances are 1.56 and 2.76 Å, respectively. The global minimum of  $\text{La}_3\text{B}_{14}^-$  can be viewed as the first inverse triple-decker consisting of two  $\text{B}_8$  rings. However, the perfect linear  $\text{La} \dots \text{B}_8 \dots \text{La} \dots \text{B}_8 \dots \text{La}$  inverse triple-decker is not stable because of the strong inter-layer B–B bonding. The transformation from this high-symmetry linear structure to the bent global minimum of  $\text{La}_3\text{B}_{14}^-$  is schematically shown in Figure 4, by tilting the two  $\text{B}_8$  rings and sharing one B–B unit. There are some structural distortions in the conjoined part of the two rings, whereas the unshared five B–B bonds on each  $\text{B}_8$  ring are very similar to those in the  $\text{La}_2\text{B}_8$  inverse sandwich, ranging from 1.53 to 1.60 Å (Figure S3). These B–B bond lengths are consistent with B=B double bonds, according to Pyykko’s covalent radii.<sup>40</sup> The multiple B–B bond order is borne out from the AdNDP analyses for  $\text{La}_3\text{B}_{14}^-$  (Figure 3), as well as for  $\text{La}_2\text{B}_8$ . In the conjoined part, the shared B–B bond has a significantly lengthened bond distance of 1.78 Å, which is consistent with a B–B single bond. The neighboring B atoms next to the shared B–B bond from both the  $\text{B}_8$  rings also form a B–B single bond (1.70 Å, Figure S3), resulting in a  $\text{B}_3$  triangle with one of the shared B atoms. The 3c-2e bonds revealed in the AdNDP analyses are largely responsible for these additional conjoined B–B bonds, which significantly enhanced the binding between the two conjoined  $\text{B}_8$  rings.

The conjoined  $\text{B}_8$  rings did not affect the bonding with the La atoms, in fact, they have enhanced the metal-ligand bonding. The  $\text{La}^b\text{-B}$  bond distances for the two outer La atoms range from

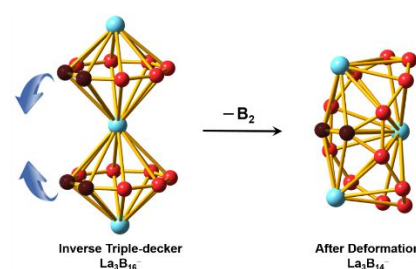


**Figure 4.** Schematics showing the transformation from a perfect linear inverse triple-decker,  $\text{La} \dots \text{B}_8 \dots \text{La} \dots \text{B}_8 \dots \text{La}$  to the global minimum, bent triple-decker of  $\text{La}_3\text{B}_{14}^-$  with two conjoined  $\text{B}_8$  rings by sharing a  $\text{B}_2$  unit (dark brown color).

2.68 to 2.78 Å, which are shorter on average than those in the  $\text{La}_2\text{B}_8$  inverse sandwich (2.76 Å). The central La atom ( $\text{La}^c$ ) also has optimal bonding with the boron framework, as shown in the AdNDP analyses discussed above. We also carried out QTAIM calculation and analyzed bond order indices to investigate the bonding of La–B and the bridged B–B unit as shown in Table S3. Compared with covalent B–B interactions, the La–B bonding is primarily of dative bonding character ( $\rho > 0$ ,  $E < 0$ ,  $\nabla^2\rho > 0$ ) with little covalent contribution. The binding energy between the three La atoms and the boron framework is calculated to be 665.15 kcal/mol at PBE0/TZP level. Overall, the high stability of the global minimum of  $\text{La}_3\text{B}_{14}^-$  is derived from both the enhanced B–B and La–B bonding, making it an exceptional inverse triple-decker complex.

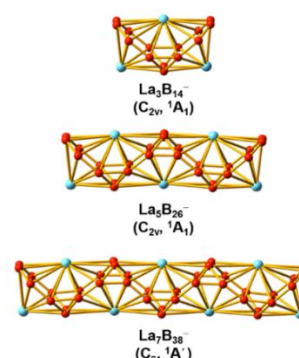


**Figure 5.** Optimized structures of  $\text{La}_5\text{B}_{26}^-$  and  $\text{La}_7\text{B}_{38}^-$  compared with that of  $\text{La}_3\text{B}_{14}^-$  at the SR-ZORA PBE/TZP level.

For transition-metal-doped boron clusters, previous studies have shown metal-centered tubular structures,<sup>16,17,19,41,42</sup> such as the  $\text{D}_{8d}\text{-Co}(\text{B}_8)_2^-$ ,  $\text{D}_{9d}\text{-Rh}(\text{B}_9)_2^-$ , and  $\text{D}_{10d}\text{-Ta}(\text{B}_{10})_2^-$ , which suggested the possibilities of metal-centered 1D boron nanotubes. The high stability of the  $\text{La}_3\text{B}_{14}^-$  tilted inverse triple-decker immediately points to a new type of 1D lanthanide-boron nanostructures by extending the triple decker with conjoint  $\text{B}_8$  rings. We have carried out preliminary calculations for two members of this series,  $\text{La}_5\text{B}_{26}^-$  consisting of four conjoint  $\text{B}_8$  rings and  $\text{La}_7\text{B}_{38}^-$  consisting of six conjoint  $\text{B}_8$  rings, as shown in Figure 5. The optimized structure of  $\text{La}_5\text{B}_{26}^-$  is closed-shell with  $\text{C}_{2v}$  ( $^1\text{A}_1$ ) symmetry and that of  $\text{La}_7\text{B}_{38}^-$  is closed-shell with  $\text{C}_s$  ( $^1\text{A}'$ ) symmetry. These 1D oligomeric nanoclusters are true minima on the potential energy surfaces

without imaginary vibrational frequencies and their Cartesian coordinates are given in Table S4. There should be a whole series of such 1D nanoclusters with the chemical formula of  $\text{La}_n\text{B}_{6n-4}^-$ . Even an infinitely long 1D nanowire may be viable or exist in new lanthanide boride compounds. Considering the fact that most of the lanthanide (Ln = La–Lu) elements can form similar inverse boron sandwiches,<sup>20</sup> we expect that they can also form similar tilted triple-deckers and 1D nanowires with tunable magnetic properties of multiple  $4f^n$  atomic centers.

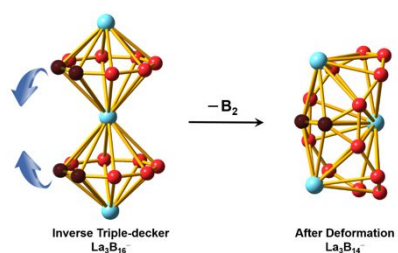
In summary, we have observed the first inverse lanthanide-boron triple-decker cluster. Photoelectron spectroscopy of  $\text{La}_3\text{B}_{14}^-$  revealed a relatively simple spectrum, suggesting a symmetric and stable structure. Theoretical calculations have shown that the global minimum of  $\text{La}_3\text{B}_{14}^-$  is closed-shell with  $C_{2v}$  symmetry, which can be viewed as a tilted inverse triple-decker with two conjoined  $\text{B}_8$  rings sharing a B–B unit due to strong inter-layer B–B bonding. Features of the  $\text{B}_8$  rings can still be recognized despite the strong inter-ring interactions. The conjoined  $\text{B}_8$  rings also enhance interactions with the La atoms, resulting in the high stability of the tilted inverse triple-decker. Extension of the tilted triple-decker can result in a series of 1D nanoclusters of the formula,  $\text{La}_n\text{B}_{6n-4}^-$ . Infinitely long 1D lanthanide-boron nanostructures consisting of conjoint  $\text{B}_8$  rings are viable with different magnetic properties or may be found in crystalline lattices of new lanthanide boride materials.

The experimental work done at Brown University was supported by the U.S. National Science Foundation (CHE-1763380). The theoretical work done at Tsinghua University was supported by the National Natural Science Foundation of China (Grant Nos. 21590792, 91426302, and 21433005). The calculations were performed using resources from the Computational Chemistry Laboratory of the Department of Chemistry under the Tsinghua Xuetang Talents Program.

## Notes and References

- A. R. Oganov, J. Chen, C. Gatti, Y. Ma, Y. Ma, C. W. Glass, Z. Liu, T. Yu, O. O. Kurakevych and V. L. Solozhenko, *Nature*, 2009, **457**, 863–867.
- B. Albert and H. Hillebrecht, *Angew. Chem. Int. Ed.*, 2009, **48**, 8640–8668.
- J. Nagamatsu, N. Nakagawa, T. Muranaka, Y. Zenitani and J. Akimitsu, *Nature*, 2001, **410**, 63–64.
- H. Y. Chung, M. B. Weinberger, J. B. Levine, A. Kavner, J. M. Yang, S. H. Tolbert and R. B. Kaner, *Science*, 2007, **316**, 436–439.
- F. Tian and Z. Ren, *Angew. Chem. Int. Ed.*, 2019, **58**, 5824–5831.
- H. J. Zhai, B. Kiran, J. Li and L. S. Wang, *Nature Mater.*, 2003, **2**, 827.
- A. N. Alexandrova, A. I. Boldyrev, H. J. Zhai and L. S. Wang, *Coord. Chem. Rev.*, 2006, **250**, 2811–2866.
- E. Oger, N. R. M. Crawford, R. Kelting, P. Weis, M. M. Kappes and R. Ahlrichs, *Angew. Chem. Int. Ed.*, 2007, **46**, 8503–8506.
- A. P. Sergeeva, I. A. Popov, Z. A. Piazza, W. L. Li, C. Romanescu, L. S. Wang and A. I. Boldyrev, *Acc. Chem. Res.*, 2014, **47**, 1349–1358.
- L. S. Wang, *Int. Rev. Phys. Chem.*, 2016, **35**, 69–142.
- Z. A. Piazza, H. S. Hu, W. L. Li, Y. F. Zhao, J. Li and L. S. Wang, *Nature Commun.*, 2014, **5**, 3113.
- H. J. Zhai, Y. F. Zhao, W. L. Li, Q. Chen, H. Bai, H. S. Hu, Z. A. Piazza, W. J. Tian, H. G. Lu, Y. B. Wu, Y. W. Mu, G. F. Wei, Z. P. Liu, J. Li, S. D. Li and L. S. Wang, *Nature Chem.*, 2014, **6**, 727.
- B. Kiran, S. Bulusu, H. J. Zhai, S. Yoo, X. C. Zeng and L. S. Wang, *Proc. Natl. Acad. Sci. (USA)*, 2005, **102**, 961–964.
- C. Romanescu, T. R. Galeev, W. L. Li, A. I. Boldyrev and L. S. Wang, *Acc. Chem. Res.*, 2012, **46**, 350–358.
- I. A. Popov, W. L. Li, Z. A. Piazza, A. I. Boldyrev and L. S. Wang, *J. Phys. Chem. A*, 2014, **118**, 8098–8105.
- I. A. Popov, T. Jian, G. V. Lopez, A. I. Boldyrev and L. S. Wang, *Nature Commun.*, 2015, **6**, 8654.
- W. L. Li, X. Chen, T. Jian, T. T. Chen, J. Li and L. S. Wang, *Nat. Rev. Chem.*, 2017, **1**, 0071.
- T. T. Chen, W. L. Li, T. Jian, X. Chen, J. Li and L. S. Wang, *Angew. Chem. Int. Ed.*, 2017, **56**, 6916–6920.
- W. L. Li, T. Jian, X. Chen, H. R. Li, T. T. Chen, X. M. Luo, S. D. Li, J. Li and L. S. Wang, *Chem. Commun.*, 2017, **53**, 1587–1590.
- W. L. Li, T. T. Chen, D. H. Xing, X. Chen, J. Li and L. S. Wang, *Proc. Natl. Acad. Sci. (USA)*, 2018, **115**, E6972–E6977.
- T. T. Chen, W. L. Li, J. Li and L. S. Wang, *Chem. Sci.*, 2019, **10**, 2534–2542.
- R. Hoffmann, *Angew. Chem. Int. Ed.*, 1982, **21**, 711–724.
- A. Fessenbecker, M. D. Attwood, R. F. Bryan, R. N. Grimes, M. K. Woode, M. Stephan, U. Zenneck and W. Siebert, *Inorg. Chem.*, 1990, **29**, 5157–5163.
- D. K. P. Ng and J. Jiang, *Chem. Soc. Rev.*, 1997, **26**, 433–442.
- V. Lorenz, S. Blaurock, C. G. Hrib and F. T. Edelmann, *Organometallics*, 2010, **29**, 4787–4789.
- A. Salzer and H. Werner, *Angew. Chem. Int. Ed.*, 1972, **11**, 930–932.
- J. W. Lauher, M. Elian, R. H. Summerville and R. Hoffmann, *J. Am. Chem. Soc.*, 1976, **98**, 3219–3224.
- H. Werner, *Angew. Chem. Int. Ed.*, 1977, **16**, 1–9.
- J. Moraczewski and W. E. Geiger Jr, *J. Am. Chem. Soc.*, 1978, **100**, 7429–7431.
- A. R. Kudinov, M. I. Rybinskaya, Y. T. Struchkov, A. I. Yanovskii and P. V. Petrovskii, *J. Organomet. Chem.*, 1987, **336**, 187–197.
- W. Siebert, J. Edwin and M. Bochmann, *Angew. Chem. Int. Ed.*, 1978, **17**, 868–869.
- E. D. Jemmis and A. C. Reddy, *Organometallics*, 1988, **7**, 1561–1564.
- D. Chabach, A. De Cian, J. Fischer, R. Weiss and M. E. M. Bibout, *Angew. Chem. Int. Ed.*, 1996, **35**, 898–899.
- J. Li, D. Gryko, R. B. Dabke, J. R. Diers, D. F. Bocian, W. G. Kuhr and J. S. Lindsey, *J. Org. Chem.*, 2000, **65**, 7379–7390.
- L. S. Wang, H. S. Cheng and J. Fan, *J. Chem. Phys.*, 1995, **102**, 9480–9493.
- Y. F. Zhao, X. Chen and J. Li, *Nano Res.*, 2017, **10**, 3407–3420.
- X. Chen, Y. F. Zhao, Y. Y. Zhang and J. Li, *J. Comput. Chem.*, 2019, **40**, 1105–1112.
- ADF, 2016.101, SCM, Theoretical Chemistry, Vrije Universiteit, Amsterdam, The Netherlands, (<http://www.scm.com>).
- D. Y. Zubarev and A. I. Boldyrev, *Phys. Chem. Chem. Phys.*, 2008, **10**, 5207–5217.
- P. Pyykkö, *J. Phys. Chem. A*, 2015, **119**, 2326–2337.
- T. Jian, W. L. Li, I. A. Popov, G. V. Lopez, X. Chen, A. I. Boldyrev, J. Li and L. S. Wang, *J. Chem. Phys.*, 2016, **144**, 154310.
- T. Jian, W. L. Li, X. Chen, T. T. Chen, G. V. Lopez, J. Li and L. S. Wang, *Chem. Sci.*, 2016, **7**, 7020–7027.

TOC graphics:



The relationship between the global minimum of tilted inverse triple-decker  $\text{La}_3\text{B}_{14}^-$  and the perfect inverse triple-decker  $\text{La}\dots\text{B}_8\dots\text{La}\dots\text{B}_8\dots\text{La}$ .